circRNA_013145-miR-185-5p-RhoA axis: A novel mechanism in the pathophysiology of diabetes-induced erectile dysfunction

WENHAN HUANG[1*], XIN LV[1*], JIAHUA QIAN[2,3], YIHAO CHEN[1], YUHE SI[2,3], JINGWEI WANG[4] and JIANXIONG MA[2,3,5]

[1]The Second Clinical Medical College, Zhejiang Chinese Medical University, Hangzhou, Zhejiang 310053, P.R. China; [2]Department of Nephrology, The First Affiliated Hospital of Zhejiang Chinese Medical University (Zhejiang Provincial Hospital of Chinese Medicine), Hangzhou, Zhejiang 310006, P.R. China; [3]The First Clinical Medical College, Zhejiang Chinese Medical University, Hangzhou, Zhejiang 310053, P.R. China; [4]Academy of Chinese Medical Sciences, Zhejiang Chinese Medical University, Hangzhou, Zhejiang 310053, P.R. China; [5]Zhejiang Key Laboratory of Research and Translation for Kidney Deficiency-Stasis-Turbidity Disease, Zhejiang Chinese Medical University, Hangzhou, Zhejiang 310053, P.R. China

Received December 22, 2025; Accepted July 2, 2026

DOI: 10.3892/ijmm.2026.5938

Abstract. Diabetes mellitus-induced erectile dysfunction (DMED) is a common diabetic complication characterized by endothelial dysfunction and corpus cavernosum (CC) remodeling. Although circular RNAs (circRNAs) have been implicated in diabetic vascular diseases, their roles in DMED remain largely unknown. The present study investigated the biological function and underlying mechanism of circRNA_013145 in DMED. CircRNA microarray analysis identified circRNA_013145 as a significantly upregulated circRNA in penile tissue from DMED rats. Its biological function was evaluated using loss-of-function and rescue experiments in high glucose (HG)-treated CC smooth muscle cells (CCSMCs), human umbilical vein endothelial cells (HUVECs) and a DMED rat model. circRNA_013145 expression was markedly increased in DMED penile tissue and HG-treated cells. circRNA_013145 knockdown attenuated HG-induced oxidative stress, inflammation, apoptosis, autophagy and phenotypic transformation, while improving endothelial function and cell viability. Mechanistically, circRNA_013145 served as a molecular sponge for miR-185-5p, thereby positively regulating RhoA expression. Rescue experiments demonstrated that inhibition of miR-185-5p partially abolished the protective effects of circRNA_013145 knockdown. Furthermore, adenovirus-mediated knockdown of circRNA_013145 significantly improved erectile function and alleviated cavernosal pathological injury in DMED rats, as evidenced by an increased intracavernosal pressure (ICP)/mean arterial pressure (MAP) ratio, enhanced CD31 expression and reduced collagen deposition. In conclusion, circRNA_013145 promotes the progression of DMED through the miR-185-5p/RhoA axis. Targeting circRNA_013145 may represent a potential therapeutic strategy for DMED.

Correspondence to: Dr Jianxiong Ma, Department of Nephrology, The First Affiliated Hospital of Zhejiang Chinese Medical University (Zhejiang Provincial Hospital of Chinese Medicine), 54 Youdian Road, Hangzhou, Zhejiang 310006, P.R. China
E-mail: daxiong1990@zcmu.edu.cn

*Contributed equally

Key words: diabetes mellitus-induced erectile dysfunction, circRNA_013145, microRNA-185-5p, RhoA; endothelial dysfunction, corpus cavernosum smooth muscle cells

Introduction

Erectile dysfunction (ED) is a common male reproductive disorder characterized by the persistent inability to attain or maintain a penile erection sufficient for satisfactory sexual performance. It markedly impairs quality of life and is typically associated with psychological distress, decreased self-esteem and impaired partner relationships (1). ED is a multifactorial disorder involving vascular, neurological, endocrine, metabolic and psychological components, which complicates both its diagnosis and treatment.

Diabetes mellitus (DM) is one of the notable risk factors for ED. Epidemiological and clinical studies have shown that patients with DM have a markedly higher risk of developing ED than non-diabetic individuals (2,3), and 35-75% of diabetic patients are affected by DM-induced ED (DMED) (4). The pathogenesis of DMED is closely associated with chronic hyperglycemia-induced endothelial injury, oxidative stress, inflammatory activation, impaired nitric oxide/cyclic guanosine monophosphate signaling and cavernosal structural remodeling (5,6). In addition to endothelial dysfunction, corpus cavernosum smooth muscle cells (CCSMCs), which represent a notable cellular component of the CC, are essential for penile relaxation and blood trapping during erection (7-9). Under diabetic or high-glucose (HG) conditions, CCSMCs may undergo phenotypic transformation from a contractile phenotype toward a synthetic phenotype, characterized by

decreased α-smooth muscle actin and desmin expression, increased osteopontin expression and enhanced proliferative and migratory activity (10,11). These pathological changes contribute to impaired cavernosal relaxation, fibrosis and erectile failure.

Circular RNAs (circRNAs) are a class of endogenous non-coding RNAs generated by back-splicing of precursor mRNAs. Owing to their covalently closed-loop structure, circRNAs are resistant to exonuclease-mediated degradation and are typically more stable than their corresponding linear transcripts (12,13). circRNAs regulate gene expression through multiple mechanisms, including acting as microRNA (miRNA or miR) sponges, interacting with RNA-binding proteins and modulating transcriptional or post-transcriptional processes (14,15). circRNAs participate in the pathogenesis of diabetes, cardiovascular disease and cancer (16-18). However, the expression profile and functional significance of circRNAs in DMED remain insufficiently characterized.

Given the key role of endothelial dysfunction and CCSMC phenotypic transformation in DMED (5,6,10,11) as well as the regulatory functions of circRNAs in vascular and metabolic diseases (16-18), the present study aimed to investigate the expression profile and functional role of circRNAs in DMED and to determine whether the circRNA_013145/miR-185-5p/RhoA axis contributes to HG-induced cavernosal cellular injury and ED.

Materials and methods

Animals and samples. Male Sprague-Dawley rats (aged 8 weeks were provided by the Animal Center of Zhejiang Chinese Medical University [weight, 200±10 g; certificate no. SYXK (ZHE) 2021-0012]. Animals were held in standard experimental conditions in a laminar flow cabinet (12/12-h light/dark cycle, 24±1˚C and 45-55% humidity) free access to food and water.

Erectile function was evaluated using the apomorphine (APO) test. APO (100 μg/kg) was injected subcutaneously into the loose skin at the back of the neck. Rats were immediately placed in individual observation cages under quiet, dimly lit conditions and monitored continuously for 30 min. A positive erectile response was defined as penile engorgement and glans swelling with visible penile body protrusion. Rats showing no erectile response during the 30 min observation period were identified as DMED. For circRNA microarray screening, rats were assigned to the control and DMED groups as previously described (19). Penile tissue from four control rats and four DMED rats were selected for circRNA microarray analysis. At the end of week 4, following the erectile function examination, rats were euthanized via CO_2 asphyxiation (at a flow rate displacing 50% of the chamber volume/min) followed by cervical dislocation, in accordance with American Veterinary Medical Association (AVMA) Guidelines for the Euthanasia of Animals (20). Penile tissue was collected, snap-frozen in liquid nitrogen (-196˚C) and preserved at -80˚C. Four penile tissue samples from each group were used for circRNA microarray labeling and hybridization.

Extraction of RNA and quality control. Using the TRIzol reagent (Invitrogen; Thermo Fisher Scientific, Inc.), total RNA was extracted from rat penile tissue according to the manufacturer's instructions. Using a ND-1000 NanoDrop instrument (Thermo Fisher Scientific, Inc.), the RNA concentrations of the samples were determined at 260 nm. RNA integrity was assessed using 1.2% denaturing agarose gel electrophoresis.

Microarray labeling and hybridization of circRNA. To enrich circular RNAs and remove linear RNAs, the RNA was digested using RNase R (Epicentre; Illumina, Inc.). By a random priming method (Arraystar Super RNA Labeling kit; Arraystar, Inc.), the enriched circular RNAs were amplified and transcribed into fluorescent complementary (c)RNA, according to the manufacturer's instructions. Next, the labeled cRNA was hybridized to an Arraystar Rat circRNA array (8x15 K; Arraystar Inc.). Following hybridization, the arrays were washed and fixed using the reagents and procedures specified in the manufacturer's protocol for the Arraystar Rat circRNA Array. The arrays were then scanned using an Agilent Scanner G2505C (Agilent Technologies, Inc.).

Microarray data collection and analysis. To extract the raw data, scanned images were imported to the Agilent Feature Extraction software (version 11.0.1.1; Agilent Technologies, Inc.). Quantile normalization of the raw data and data processing were performed using the limma package in R software (version 4.4.0; R Foundation for Statistical Computing; www.r-project.org). Volcano plot filtering was used to pinpoint differentially expressed circRNAs exhibiting statistically significant variances. circRNAs with $P<0.05$ and fold-change ≥2.0 were identified as significantly differentially expressed circRNAs. To identify distinguishable circRNA expression patterns between samples, hierarchical clustering was performed using R software.

Construction of the circRNA-miRNA-mRNA regulatory network. Based on TargetScan (version 7.2; targetscan.org/mmu_72/) (21) and miRanda (version 5.1; microrna.org/) (22) and using the Arraystar homemade miRNA target prediction software (Arraystar, Inc.) provided with the Arraystar circRNA microarray analysis service, potential circRNA-miRNA interactions involving circRNA_013145 were predicted. For all comparisons, differentially expressed circRNAs were annotated using information on circRNA-miRNA interactions. A circRNA-miRNA-mRNA regulatory network was constructed using TargetScan and miRWalk (version 3.0; mirwalk.umm.uni-heidelberg.de/) (23). This network was visualized using Cytoscape (version 3.6.1; cytoscape.org/).

Gene Ontology (GO) and pathway enrichment analysis. To analyze the key circRNA_013145 functional pathways, miR-185-5p-targeting genes in the circRNA-miRNA-mRNA regulation network were assessed via Kyoto Encyclopedia of Genes and Genomes (KEGG; genome.jp/kegg/) pathway enrichment analyses and GO annotation (geneontology.org) using the Metascape database (metascape.org/) (24). For GO analyses, biological processes, molecular functions and cellular components with $P<0.05$ were considered significantly enriched.

Protein-protein interaction (PPI) network construction and analyses. Based on miR-185-5p-targeting genes, a PPI network was constructed using the species *Rattus norvegicus* and the

Search Tool for the Retrieval of Interacting Genes database (STRING, version 11.0, string-db.org/) (25) was used. Where the confidence score was ≥0.4, genes were imported into Cytoscape (version 3.6.1; cytoscape.org) for visualization. The topological parameters of the network were analyzed to identify hub genes using Network Analyzer plugins in Cytoscape. The number of direct connections with other nodes in the PPI network was considered the degree of each node. To visualize node size, the degree value was used and hub genes for miR-185-5p were defined as genes with a degree value greater than the median degree value for all nodes.

Cell culture. Primary CCSMCs were isolated from the CC of healthy male rats (age, 8 weeks) as previously described (8,26). The HUVECs were an immortalized cell line obtained from the Shanghai Institute of Biological Sciences, Chinese Academy of Sciences (cat. no. CBP60340). Cells passaged 4-8 times were divided into the following groups: HG (30 mM glucose), mannitol (5 mM glucose + 25 mM mannitol) and low-glucose (5 mM glucose). The cells were cultivated in DMEM with 10% fetal bovine serum (both Gibco; Thermo Fisher Scientific, Inc.) in a 5% CO_2 environment at 37˚C.

Cell transfection. miR-185-5p mimics and inhibitors were obtained from Guangzhou RiboBio Co., Ltd. The sequences were as follows: miR-185-5p mimic (duplex), sense, 5'-UGG AGAGAAAGGCAGUUCCUGA-3' and antisense, 5'-UCA GGAACUGCCUUUCUCUCCA-3'; and miR-185-5p inhibitor (chemically modified single-stranded antisense oligonucleotide), 5'-UCAGGAACUGCCUUUCUCUCCA-3'. The mimic sense strand is identical to the mature miR-185-5p sequence, whereas the mimic antisense strand and inhibitor are reverse-complementary antisense oligonucleotides.

Short interfering (si)RNAs targeting circRNA_013145 and the negative control (si-NC) were generated by Shanghai GenePharma Co., Ltd. The siRNAs targeting circRNA_013145 were designed to span the Exon3-Exon2 back-splice junction. The targeting sequences were as follows: si-Circ#1, 5'-TTA TTAGAGGCAAAGCACGGA-3'; si-Circ#2, 5'-TATTAGAGG CAAAGCACGGAG-3' and si-Circ#3, 5'-TTTATTAGAGGC AAAGCACGG-3'. The sequence of si-NC was 5'-UUCUCC GAACGUGUCACGU-3'. The same siRNA sequences were used in CCSMCs and HUVECs after confirming conservation of the targeted region.

The targeting portions of the adenovirus-delivered short hairpin (sh)RNA targeting circRNA_013145 (Ad-sh_circRNA_013145) and Ad-sh_NC were 5'-TTATTAGAGGCA AAGCACGGA-3' and 5'-TTCTCCGAACGTGTCACGT-3', respectively (Table SI). The overlap between the siRNA/shRNA target sites and the circRNA_013145 back-splice junction is shown in Fig. S1.

Briefly, CCSMCs and HUVECs were transfected with si-circRNA_013145, si-Circ_NC, miR-185-5p inhibitor, miR-185-5p mimic or the corresponding NC using Lipofectamine 3000 (Invitrogen; Thermo Fisher Scientific, Inc.). For siRNA transfection, cells were transfected with 100 nM si-circRNA_013145 or si-Circ_NC. For miRNA transfection, cells were transfected with 50 nM miR-185-5p mimic, 100 nM miR-185-5p inhibitor or the corresponding miR-NC. Transfection was performed at 37˚C for 6 h, after which the medium was replaced with complete medium. Subsequent experiments were performed 24-48 h after transfection. The efficiencies of si-circRNA_013145, miR-185-5p mimic, and miR-185-5p inhibitor were confirmed by reverse transcription-quantitative (RT-q)PCR at 24 h after transfection.

RT-qPCR. Total RNA was extracted from rat penile tissue, CCSMCs and HUVECs using TRIzol (Thermo Fisher Scientific, Inc.). For circRNA_013145, linear aspartate β-hydroxylase (Asph) and RhoA amplification, total RNA was reverse-transcribed into cDNA using a PrimeScript II 1st Strand cDNA Synthesis kit (Takara Biotechnology Co., Ltd.) according to the manufacturer's instructions. Divergent primers spanning the Exon3-Exon2 back-splice junction were used to amplify circRNA_013145, whereas convergent primers were used to detect linear Asph and RhoA mRNAs. qPCR was performed using SYBR Premix Ex Taq™ (Takara Biotechnology Co., Ltd.) on an ABI 7500 system (Applied Biosystems; Thermo Fisher Scientific, Inc.). The thermocycling conditions were as follows: initial denaturation at 95˚C for 30 sec, followed by 40 cycles of denaturation at 95˚C for 5 sec and annealing/extension at 60˚C for 34 sec.

For miR-185-5p quantification, total RNA was reverse-transcribed into cDNA using a Mir-X™ miRNA First-Strand Synthesis kit (Takara Bio, Inc.) according to the manufacturer's instructions. RT-qPCR was performed using a miR-185-5p-specific forward primer and the universal mRQ 3' primer supplied with the Mir-X™ miRNA First-Strand Synthesis kit. RT-qPCR was performed using SYBR Premix Ex Taq™ (Takara Biotechnology Co., Ltd.) on an ABI 7500 system (Applied Biosystems, Thermo Fisher Scientific, Inc.). U6 and GAPDH were used as internal controls for miRNA and mRNA/circRNA quantification, respectively. Relative RNA expression was calculated using the $2^{-\Delta\Delta Cq}$ method (27). Primer sequences are listed in Table SII.

Actinomycin D and RNase R treatment. Total RNA (5 μg) from CCSMCs and HUVECs was incubated with 4 U/μg RNase R (Epicentre Technologies) for 30 min at 37˚C. DMSO or 2 μg/ml actinomycin D (Sigma-Aldrich; Merck KGaA) was added to cells at 37˚C for 0, 6, 12, 18 and 24 h. Asph and circRNA_013145 RNA expression was determined by RT-qPCR, as aforementioned.

Nuclear and cytoplasmic fractionation. CCSMCs and HUVECs were detached using 0.25% trypsin-EDTA (Gibco; Thermo Fisher Scientific, Inc.), resuspended, washed with 1,000 μl PBS and centrifuged at 300 x g for 5 min at 4˚C. NE-PER Nuclear and Cytoplasmic Extraction Reagent kits (cat.no. 78833; Thermo Fisher Scientific, Inc.) were used to isolate nuclear and cytoplasmic fractions according to the manufacturer's instructions. Using the QIAamp RNA Mini kit (cat.no. 52904; Qiagen, Inc.), total RNA was extracted according to the manufacturer's instructions. U6- and GAPDH-processed mRNAs in isolated RNA were detected as controls for nuclear and cytoplasmic RNA, respectively. circRNA_013145 expression was assessed using RT-qPCR, as aforementioned.

Fluorescence in situ hybridization (FISH). FISH was performed using custom-designed fluorescent probes specific for circRNA_013145 and miR-185-5p (Guangzhou BersinBio Co., Ltd.). The miR-185-5p probe was labeled with fluorescein isothiocyanate (FITC), whereas the circRNA_013145 probe was labeled with Cy5. Briefly, CCSMCs and HUVECs were fixed with 4% paraformaldehyde at room temperature for 20 min. Cells were treated with proteinase K (20 μg/ml) at 37˚C for 10 min according to the manufacturer's protocol. The probes were mixed with hybridization solution at a ratio of 1:39, denatured at 75˚C for 5-8 min, and hybridized overnight at 37˚C (16-20 h). After hybridization, cells were washed sequentially with 2x saline-sodium citrate (SSC) buffer at 53˚C for 5 min, 0.1% NP-40/2xSSC buffer at 42˚C for 5 min and 2X SSC buffer at 42˚C for 5 min. Nuclei were counterstained with DAPI at room temperature for 10 min. Images were captured using an inverted fluorescence microscope (DMI 3000 B; Leica GmbH).

Cell Counting Kit-8 (CCK-8). Cell viability was evaluated using a CCK-8 kit (cat. no. C0037; Beyotime Biotechnology). Transfected CCSMCs and HUVECs ($1x10^4$ cells/well) were seeded onto 96-well plates. After culturing at 37˚C in a 5% CO_2 incubator for 24 h under HG conditions, the culture medium was replaced with fresh HG DMEM (Gibco; Thermo Fisher Scientific, Inc.) containing 10% CCK-8. Following incubation at 37˚C for 2 h, absorbance at 450 nm was determined using a spectrophotometer (Varioskan LUX, Thermo Fisher Scientific, Inc.).

ELISA and biochemical assays. The concentrations of the inflammatory factors IL-6 and TNF-α in the supernatant of HG-treated, transfected CCSMCs and HUVECs were measured using commercial ELISA kits according to the manufacturers' instructions (Beyotime Biotechnology). For CCSMCs, Rat IL-6 ELISA kit (cat. no. PI328; Beyotime Biotechnology) and Rat TNF-α ELISA kit (cat. no. PT516; Beyotime Biotechnology) were used. For HUVECs, Human IL-6 ELISA kit (cat. no. PI330; Beyotime Biotechnology) and Human TNF-α ELISA kit (cat. no. PT518; Beyotime Biotechnology) were used. Cell culture supernatants were collected and centrifuged at 1,000 x g for 5 min at 4˚C to remove cell debris before detection.

For the assessment of oxidative stress-related indicators, cells were lysed using the sample preparation buffer in the corresponding assay kit, according to the manufacturers' instructions. Cell lysates were centrifuged at 16,000 x g for 15 min at 4˚C, and the supernatants were collected. MDA levels were measured using a Lipid Peroxidation MDA Assay Kit (cat. no. S0131S; Beyotime Biotechnology). Total SOD activity was measured using a Total Superoxide Dismutase Assay Kit with WST-8 (cat. no. S0101S; Beyotime Biotechnology). Total NO levels were measured using a Total Nitric Oxide Assay Kit (cat. no. S0024; Beyotime Biotechnology). cGMP levels were measured using species-specific cGMP ELISA kits: Human cGMP ELISA kit (cat. no. CB10702-Hu; CUSABIO Technology LLC) for HUVECs and Rat cGMP ELISA kit (cat. no. CB10438-Ra; CUSABIO Technology LLC) for CCSMCs. All assays were performed according to the manufacturers' instructions.

Mitochondrial ROS detection. Mitochondrial ROS) levels were assessed using MitoSOX Green mitochondrial superoxide indicator (cat. no. M36006; Thermo Fisher Scientific, Inc.) according to the manufacturer's instructions. Briefly, CCSMCs and HUVECs were incubated with MitoSOX Green working solution diluted at 1:1,000 at 37˚C in the dark, washed with PBS and observed using an inverted fluorescence microscope (DMI 3000 B; Leica GmbH). Green fluorescence intensity was used to indicate mitochondrial ROS levels.

Colony formation assay. Following transfection with 100 nM si-Circ_#1 or si-Circ_NC, CCSMCs and HUVECs were cultured in DMEM supplemented with 10% FBS at 37˚C in a 5% CO_2 incubator. Transfected cells ($5x10^2$ cells/well) were seeded onto 6-well plates and cultured at 37˚C for 10 days. Following removal of the medium, cell colonies were fixed with 4% paraformaldehyde at room temperature for 20 min and stained for 30 min with 0.5% crystal violet solution at room temperature. Colonies were defined as clusters containing >50 cells and were counted manually under a light microscope. Images were captured using a light microscope. All experiments were performed in triplicate.

Flow cytometry. CCSMC and HUVEC apoptosis rates were measured using the Annexin V-FITC Apoptosis Assay kit (cat. no. C1062S; Beyotime Biotechnology). Briefly, transfected CCSMCs and HUVECs were seeded onto 6-well plates and cultured under HG conditions at 37˚C for 48 h. Following harvest, the cells underwent two cold PBS washes before addition of 10 μl propidium iodide and 5 μl Annexin V reagent in the dark at room temperature for 15 min. Apoptosis rate was determined using a FACSCalibur flow cytometer (BD Biosciences), and data were analyzed using FlowJo software (version 10.9.0). The apoptosis rate was calculated as the percentage of early and late apoptotic cells.

Wound healing assay. Transfected CCSMCs and HUVECs were plated onto 6-well plates ($5x10^5$ cells/well) and incubated at 37˚C in a 5% CO_2-containing environment until 100% confluence was attained. Next, a linear wound was generated using a 200 μl pipette tip. Following washing with PBS to remove detached cells, the cells were incubated in serum-free HG DMEM at 37˚C for 24 h. Images were captured at 0 and 24 h using an inverted light microscope. The migration distance was analyzed using Image Pro Plus 6.0 software (Media Cybernetics Inc.).

Immunofluorescence staining. Transfected CCSMCs that were fixed in 4% paraformaldehyde for 20 min, rinsed with PBS, permeabilized with 0.5% Triton X-100 in PBS for 15 min and blocked with 10% bovine serum albumin at room temperature for 1 h. Next, the cells were exposed to primary antibodies for α-smooth muscle actin (SMA; 1:200, cat. no. ab223068), desmin (1:100; cat. no. ab227651) and osteopontin (1:1,000, cat. no. ab8448) at 4˚C overnight, then incubated for 1 h at room temperature with secondary antibodies (Alexa Fluor® 488-conjugated goat anti-rabbit IgG, 1:1,000, cat. no. ab150077; Abcam). Images were captured using an inverted fluorescence microscope (DMI 3000 B; Leica GmbH) and analyzed using ImageJ software (version 1.53t; National Institutes of Health.

Luciferase reporter assay. The circRNA_013145 fragment containing the predicted miR-185-5p binding site and the RhoA 3'-UTR fragment containing the predicted miR-185-5p binding site were synthesized by Sangon Biotech. The corresponding mutant fragments with mutations in the miR-185-5p seed-binding regions were also synthesized. The wild-type (WT) and mutant (Mut) fragments were subcloned into the psiCHECK-2 reporter vector (Promega Corporation) to generate WT-circRNA_013145, Mut-circRNA_013145, WT-RhoA and Mut-RhoA reporter constructs. The sequences of the miR-185-5p mimic, miR-185-5p inhibitor and corresponding negative controls are listed in Table SI. CCSMCs and HUVECs ($5x10^4$ cells/well) were seeded onto 24-well plates and co-transfected with the reporter constructs and miR-185-5p mimic or miR-NC using Lipofectamine 3000 (Invitrogen; Thermo Fisher Scientific, Inc.). At 24 h after transfection, luciferase activity was measured using the Dual-Luciferase Reporter Assay System (Promega Corporation) according to the manufacturer's instructions. Relative luciferase activity was normalized to the internal control luciferase activity from the psiCHECK-2 vector.

RNA immunoprecipitation (RIP) assay. RIP was performed using a Magna RIP RNA-Binding Protein Immunoprecipitation kit (MilliporeSigma) according to the manufacturer's instructions. Briefly, CCSMCs and HUVECs were lysed in RIP lysis buffer supplemented with RNase inhibitors and protease inhibitors. Cell lysates were cleared by centrifugation at 12,000 x g for 10 min at 4˚C and 100 μl cell lysate was used for each reaction. Magnetic beads were incubated with 5 μg anti-Argonaute 2 (Ago2; cat. no. ab156870) or 5 μg normal IgG antibody (cat. no. ab181236; both Abcam). The antibody-conjugated magnetic beads were then incubated with cell lysates at 4˚C overnight. RNA-protein complexes were isolated by magnetic separation and washed according to the manufacturer's protocol. Immunoprecipitated RNAs were purified and analyzed by qPCR to detect circRNA_013145, miR-185-5p and RhoA, as aforementioned.

Western blot assay. Transfected CCSMCs, HUVECs and penile tissues were lysed in ice-cold RIPA buffer (Beyotime Biotechnology) containing protease inhibitors (Sigma-Aldrich; Merck KGaA). The amount of protein in the supernatant was determined using a BCA kit. Next, equal amounts of protein (30 μg/lane) were separated by 8-12% SDS-PAGE and transferred onto PVDF membranes. After being blocked with 5% non-fat milk at room temperature for 2 h, the membranes were incubated with primary antibodies overnight at 4˚C. The primary antibodies were as follows: against β-actin (cat. no. AF7018), GAPDH (1:3,000; cat. no. AF7021), Bax (cat. no. AF0120), endothelial nitric oxide synthase (eNOS) (1:3,000; cat. no. AF0096), p62 (cat. no. AF5384), Beclin-1 (cat. no. AF5128), LC3-I/II (1:2,000, cat. no. AF5402), Caspase-9 (cat. no. AF6348), Caspase-3 (cat. no. AF6311), Bcl-2 (cat. no. AF6139), protein kinase G (PKG) (cat. no. DF7018), vascular cell adhesion molecule-1 (VCAM1; cat. no. DF7306), ICAM-1 (cat. no. AF6088), RhoA (cat. no. AF6352; all Affinity Biosciences), α-SMA (all 1:2,000, cat. no. ab223068), desmin (1:100, cat. no. ab227651) and osteopontin (1:1,000; cat. no. ab8448; all Abcam. The membranes were then incubated with horseradish peroxidase (HRP)-conjugated goat anti-rabbit IgG secondary antibody (1:5,000; cat. no. S0001; Affinity Biosciences) for 2 h at room temperature. Following washing, protein bands were detected using the BeyoECL Plus reagent (Beyotime Biotechnology). ImageJ (version 1.53t; National Institutes of Health) was used to calculate band intensity.

Functional assessment of circRNA_013145 knockdown in vivo. A total of 60 6-week-old Sprague-Dawley male rats (weight, 200±20 g) were provided by Shanghai SLAC Laboratory Animal Co., Ltd. Animals were housed under standard laboratory conditions with a 12/12-h light/dark cycle, temperature of 24±1˚C and humidity of 45-55%, with free access to food and water. After 1 week adaptive feeding, all rats were subjected to overnight fasting and 50 rats were intraperitoneally injected streptozotocin (60 mg/kg, Sigma-Aldrich; Merck KGaA) to induce DM. The remaining 10 rats were intraperitoneally injected 0.1 mol/l citrate-phosphate buffer (pH 4.5) and used as control rats. After 72 h, a blood glucose meter (ACCU-CHEK Performa; Roche Diagnostics) was used to monitor the blood glucose levels of rats. Diabetes was diagnosed based on fasting blood glucose >16.7 mmol/l.

To evaluate erectile function, after 10 weeks, an APO-induced erection test was performed in the DM rats. In total, 35 rats with DMED were randomly divided into the DMED-Ad-NC (n=12), DMED (n=11) and DMED-Ad-sh_circRNA_013145 (n=12) groups. Recombinant Ad-circRNA_013145 shRNA (titer, $5.6x10^9$ plaque-forming units (PFU)/ml] and NC Ad-null shRNA (titer, $6.4x10^9$ pfu/ml) were purchased from Shanghai GenePharma Co., Ltd. For *in vivo* knockdown, rats in the DMED-Ad-sh_circRNA_013145 group received intracavernosal injections of Ad-circRNA_013145 shRNA (20 μl). Rats in the DMED-Ad-NC group received equal volumes of Ad-null shRNA. Control and DMED rats received saline (20 μl). Injections were performed using a 30-gauge insulin needle inserted into the CC at the mid-penile level. The needle was inserted laterally to avoid the dorsal neurovascular bundle, and the solution was injected over 30 sec. Injections were repeated daily for 4 consecutive weeks.

Erectile function and pathological changes in DMED rats following Ad-mediated intervention were evaluated as previously described (19). Briefly, following 4 weeks of treatment, the animals were administered APO (100 μg/kg) through injection into the neck skin and placed under observation for 30 min. Erection was assessed based on hyperemia of the penile head, penile swelling, receding prepuce and ejaculation. If no erectile response was observed within the 30-min observation period, erectile latency was recorded as 30 min.

Using a four-channel acquisition system (cat. no. BL420S; Chengdu Techman Software Co. Ltd.), all animals were subjected to a cavernosometric test to measure mean arterial pressure (MAP) and maximal intracavernosal pressure (max ICP).

Penile tissues were collected, fixed with 4% paraformaldehyde at 4˚C for 24 h, embedded in paraffin and sectioned at a thickness of 5 μm. Hematoxylin and eosin (H&E) staining was performed to evaluate the histological morphology and vascular structures. For H&E staining, sections were stained with Mayer's hematoxylin for 10 min at room temperature,

rinsed, differentiated in 1% HCl/70% ethanol for 5 sec, rinsed in running tap water for 10 min, and then incubated with eosin working solution for 15 sec. Masson's trichrome staining was performed to assess collagen deposition and smooth muscle content. The staining procedure was as follows: Weigert's iron hematoxylin for 10 min, Biebrich scarlet-acid fuchsin solution for 15 min, phosphomolybdic-phosphotungstic acid solution for 10 min, aniline blue solution for 10 min; 1% acetic acid for 3 min; dehydrated through graded ethanol, cleared in xylene, and mounted with neutral resin (all at room temperature). Images were captured using a light microscope, and quantitative analysis of collagen deposition and smooth muscle content was performed using ImageJ software (version 1.53t; National Institutes of Health).

Apoptosis in CC tissue was assessed using a One Step TUNEL Apoptosis Assay kit (cat. no. C1086; Beyotime Biotechnology) according to the manufacturer's instructions. Briefly, paraffin-embedded penile tissue sections were deparaffinized, rehydrated, permeabilized and incubated with TUNEL reaction mixture at 37˚C for 60 min in the dark. After washing with PBS, nuclei were counterstained with DAPI, and images were captured using a fluorescence microscope. The apoptosis level was quantified as the percentage of TUNEL-positive cells.

Vascular structures in the CC were evaluated by CD31 immunofluorescence staining. Briefly, paraffin-embedded penile tissue sections were deparaffinized, rehydrated, subjected to antigen retrieval and blocked. The sections were incubated with anti-CD31 primary antibody (1:200; cat. no. ab182981; Abcam) at 4˚C overnight, followed by incubation with fluorescent secondary antibody at room temperature for 1 h. Nuclei were counterstained with DAPI, and images were captured using a fluorescence microscope. The number of CD31-positive vessels in the CC was quantified. The target gene and protein levels were determined by RT-qPCR and western blotting, respectively, as aforementioned.

Statistical analysis. All data are expressed as the mean ± SD. All statistical analyses were performed using GraphPad Prism 5.0 (Dotmatics) and SPSS (version 22.0; IBM Corp.). Differences were compared using an unpaired two-tailed Student's t-test or one-way ANOVA with Tukey's post hoc test. $P<0.05$ was considered to indicate a statistically significant difference. All experiments were repeated ≥3 times independently.

Results

Differential circRNA expression profile in penile tissue of DMED rats. The median normalized circRNA expression values of different samples were similar following normalization, suggesting comparable data distribution across samples (Fig. S2A). Differences in circRNA expression between the DMED and control groups are displayed in scatter plots (Fig. S2B). In total, 1,288 differentially expressed circRNAs were identified, including 647 down- and 641 upregulated circRNAs (Table SIII). A volcano plot revealed differentially expressed circRNAs between the DMED and control groups, with an absolute fold-change value ≥2 and $P<0.05$ (Fig. S2C). Distinctive patterns of circRNA expression were identified by hierarchical clustering (Fig. S2D).

Validation of differentially expressed circRNAs. RT-qPCR analysis was performed to confirm the circRNA microarray results on the five most up- and downregulated circRNAs in the penile tissue samples of control and DMED rats (Table SIV). Consistent with microarray findings, relative circRNA_013145, circRNA_008695, circRNA_010964 and circRNA_31436 expression was significantly upregulated in rats with DMED compared with control rats (Fig. S3A-D). No difference was observed in the relative expression of circRNA_013139 and circRNA_010502 (Fig. S3E and F). Furthermore, circRNA_26971, circRNA_003748, circRNA_011493 and circRNA_012403 expression decreased in the DMED group in comparison with the controls (Fig. S3G-J).

circRNA-miRNA interaction analysis. To identify potential circRNA-miRNA interactions in rats with DMED, circRNA_013145 was selected for bioinformatics analyses and prediction. circRNA_013145 was predicted to harbor binding sites for rno-miR-185-5p, rno-miR-759, rno-miR-217-3p, rno-miR-1843b-5p and rno-miR-3594-5p. Fig. S4 displays the MRE sequence analysis. A circRNA-miRNA-mRNA interaction network was constructed using Cytoscape based on the predicted target genes of miRNAs that are targeted by circRNA_013145 (Fig. S5).

Functional enrichment analysis and PPI network construction. Recent studies have implicated miR-185-5p in HG-induced cell injury and diabetic complications (28,29). Therefore, miR-185-5p was selected for downstream enrichment and network analyses. Based on its target genes, GO and KEGG pathway enrichment analyses were performed.

GO enrichment analysis showed that target genes for miR-185-5p were enriched in biological processes including 'cellular response to peptide' and 'Ras protein signal transduction' (Fig. S6A), molecular functions including 'protein C-terminus binding' and 'ion channel binding' (Fig. S6B) and cellular components including 'synaptic membrane' and 'presynapses' (Fig. S6C).

KEGG pathway enrichment analysis showed enrichment of miR-185-5p target genes in 'cGMP-PKG signaling pathway' and 'cAMP signaling pathway' (Fig. S6D). Based on data from the STRING database, a PPI network of miR-185-5p target genes was constructed (Fig. S6E). In total, five hub genes were identified: RhoA, dynamin 1, growth factor receptor-bound protein 2, glutamate ionotropic receptor NMDA type subunit 2A and synapsin I.

Characterization of circRNA_013145 in HG-induced CCSMCs and HUVECs. Using microarray analyses, the present study identified circRNA_013145 as one of the most differentially expressed circRNAs (Chr 5:27,486,600-27,495,516); it originates from exons 2 and 3 of the Asph gene (Fig. 1A). qPCR showed a significant upregulation of circRNA_013145 expression in HG-induced CCSMCs and HUVECs (Fig. 1B).

Actinomycin D assay revealed circRNA_013145 to be more stable in its circular than in its linear form in CCSMCs and HUVECs (Fig. 1C). RNase R treatment digested linear

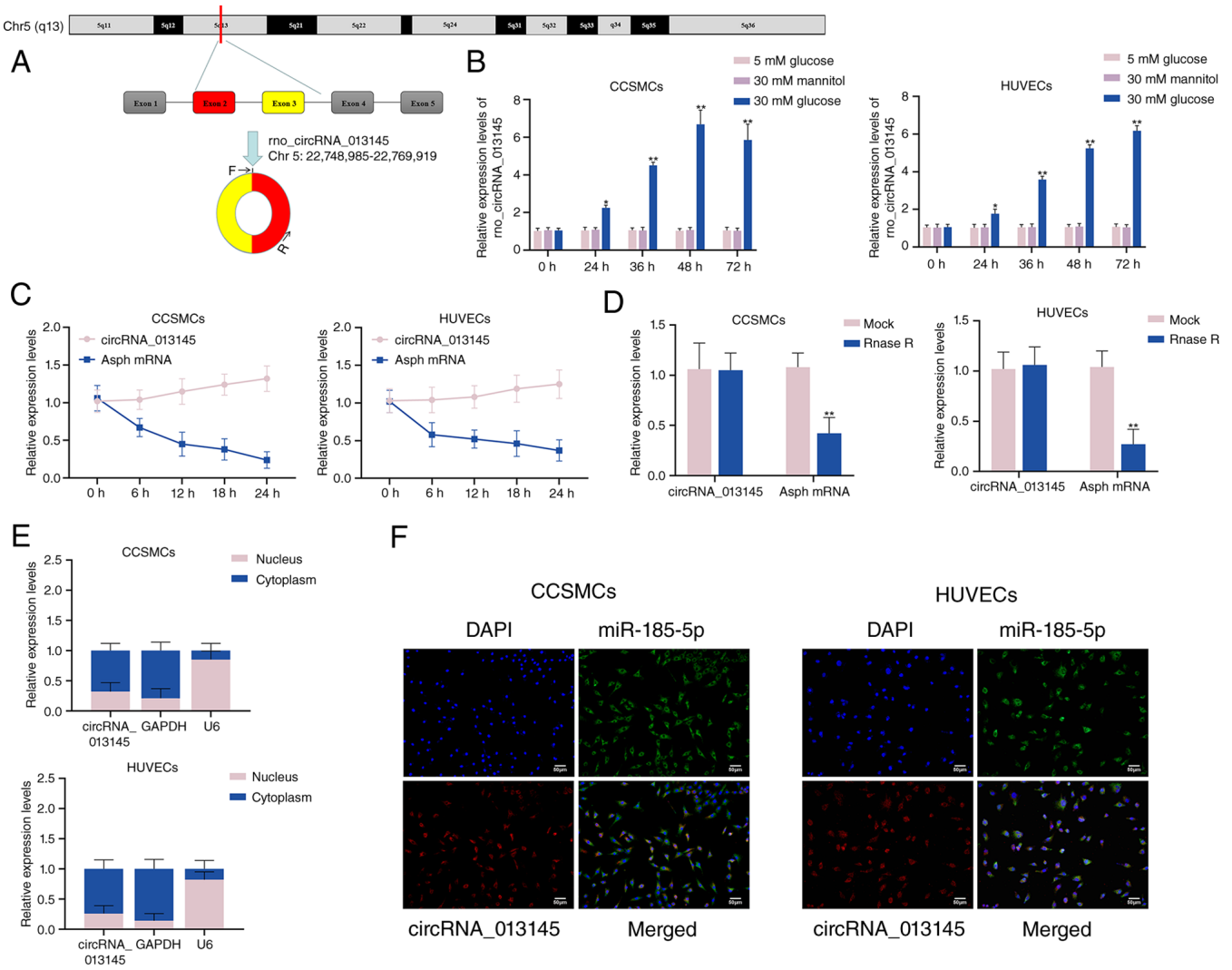

Figure 1. Expression and cell distribution of circRNA_013145 in CCSMCs and HUVECs. (A) Schematic of Asph exons 2-3 used to form circRNA_013145. (B) Expression of circRNA_013145 in CCSMCs and HUVECs. (C) Relative expression of circRNA_013145 and Asph mRNA in CCSMCs and HUVECs treated with actinomycin D at various time points. (D) circRNA_013145 resistance to RNase R treatment in CCSMCs and HUVECs. (E) Relative expression of circRNA_013145 in the nuclei and cytoplasm of CCSMCs and HUVECs was determined via reverse transcription-quantitative PCR. (F) Expression of circRNA_013145 in CCSMCs and HUVECs was determined via fluorescence *in situ* hybridization. Scale bar, 50 μm. *P<0.05, **P<0.01. circ, circular; CCSMC, corpus cavernosum smooth muscle cell; HUVEC, human umbilical vein endothelial cell; Asph, aspartate β-hydroxylase; miR, microRNA; Chr, chromosome.

Asph mRNA but not circRNA_013145 (Fig. 1D), confirming its circular structure and distinguishing it from its linear host transcript.

RT-qPCR analysis of nuclear and cytoplasmic RNA, as well as FISH, indicated that circRNA_013145 was primarily localized in the cytoplasm (Fig. 1E and F). Collectively, these findings suggested that circRNA_013145 existed as a stable cytoplasmic circRNA in CCSMCs and HUVECs.

circRNA_013145 knockdown improves cell viability and decreases inflammation and oxidative stress. Knockdown efficiencies of si-Circ#1, si-Circ#2, and si-Circ#3 were validated after transfection alone. In both CCSMCs and HUVECs, all three siRNAs significantly decreased circRNA_013145 expression compared with si-NC, with si-Circ#1 showing the strongest knockdown efficiency (Fig. S7A and B). Loss-of-function assays were performed to explore the role of circRNA_013145 in DMED progression. CCSMCs and HUVECs were transfected with siRNAs to achieve circRNA_013145 knockdown, as confirmed via qPCR analyses (Fig. 2A). Functionally, the CCK-8 assay demonstrated that, compared with the si-Circ_NC, si-Circ_#1 improved viability in HG-treated CCSMCs and HUVECs (Fig. 2B).

Moreover, circRNA_013145 knockdown significantly decreased levels of TNF-α, IL-6 and MDA, while increasing the levels of SOD, NO and cGMP in HG-treated CCSMCs and HUVECs (Fig. 2C-G). circRNA_013145 knockdown decreased mitochondrial reactive oxygen species levels (Fig. 2H). These findings indicate that circRNA_013145 knockdown attenuated inflammation and oxidative stress, thereby improving cell viability in HG-induced CCSMCs and HUVECs.

Effects of circRNA_013145 knockdown on phenotypic transformation and apoptosis in vitro. The impacts of circRNA_013145 knockdown on apoptosis, migration and cell proliferation were investigated *in vitro* by transfecting siRNA circRNA_013145 into CCSMCs and HUVECs. The number of CCSMC colonies was significantly higher in the

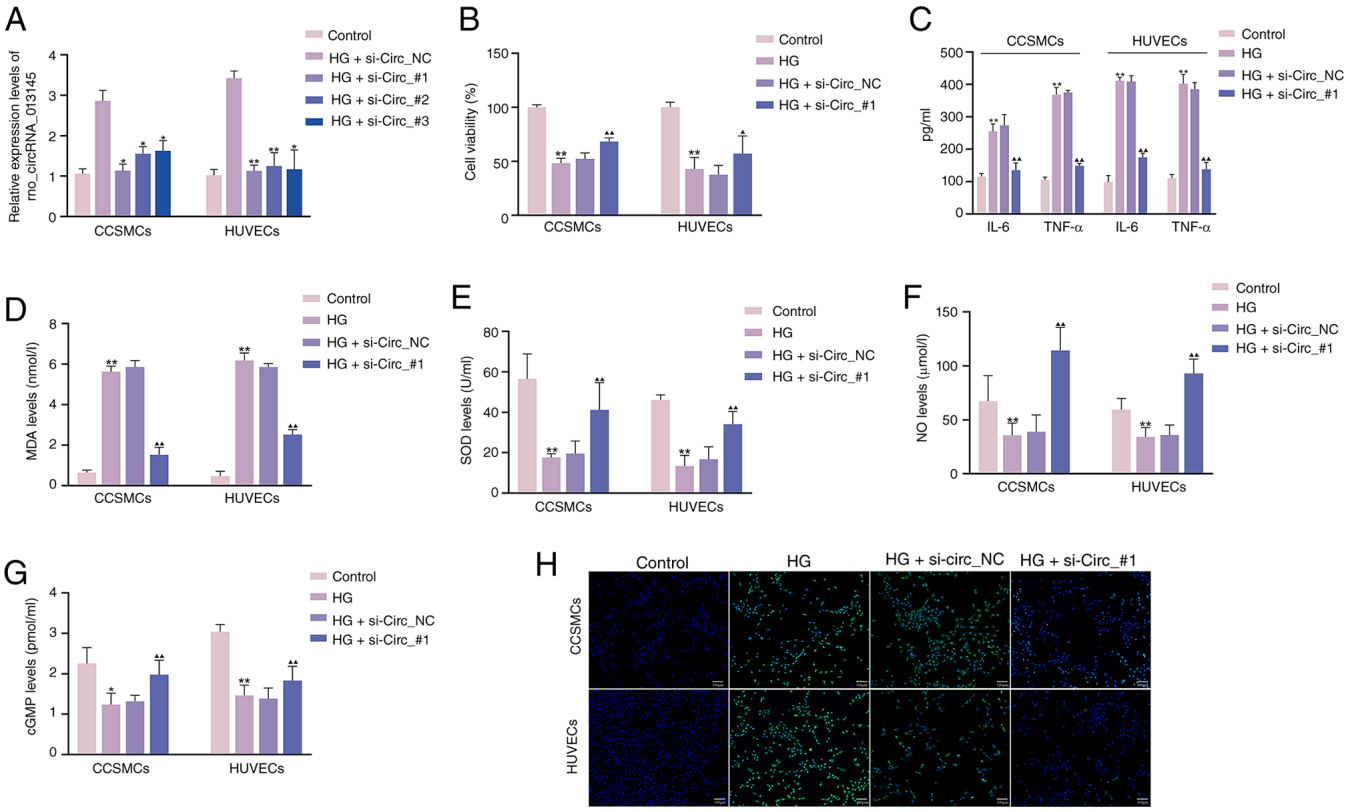

Figure 2. Effects of circRNA_013145 knockdown on cell viability, inflammation and oxidative stress in CCSMCs and HUVECs. (A) circRNA_013145 levels in si-circ_013145-transfected CCSMCs and HUVECs. (B) Effects of circRNA_013145 knockdown on cell viability as determined via the Cell Counting Kit-8 assay. (C) TNF-α, IL-6, (D) MDA, (E) SOD, (F) NO and (G) cGMP levels in circRNA_013145 silenced CCSMCs and HUVECs, as determined via ELISA. (H) Mitochondrial reactive oxygen species levels in CCSMCs and HUVECs, as determined via immunofluorescence. Magnification, x100; scale bar, 100 μm. *P<0.05, **P<0.01 vs. control; $^{▲}$P<0.05, $^{▲▲}$P<0.01 vs. si-circ_NC. circ, circular; CCSMC, corpus cavernosum smooth muscle cells; HUVECs, human umbilical vein endothelial cells; MDA, malondialdehyde; SOD, superoxide dismutase; NO, nitric oxide; c, cyclic; si, small interfering; NC, negative control; HG, high-glucose.

HG + si-Circ_NC group than in the HG + si-Circ_#1 group (Fig. 3A). Conversely, circRNA_013145 knockdown promoted HUVEC proliferation. Wound healing assay demonstrated circRNA_013145 knockdown inhibited CCSMC but enhanced HUVEC migration (Fig. 3B).

Flow cytometry showed that circRNA_013145 knockdown significantly inhibited apoptosis in both CCSMCs and HUVECs (Fig. 3C). Immunofluorescence and western blotting were performed to investigate phenotypic transformation/apoptosis-related protein expression. Immunofluorescence staining showed that circRNA_013145 knockdown increased the expression of the contractile markers α-SMA and desmin, while decreasing the expression of the synthetic marker osteopontin in HG-induced CCSMCs (Fig. 4A), suggesting attenuation of CCSMC phenotypic transformation. Western blotting showed that si-Circ#1 increased p62, PKG, and Bcl-2 levels and decreased Beclin-1, Caspase-9, LC3-II/LC3-I, Bax and Caspase-3 levels in CCSMCs. In HUVECs, circRNA_013145 knockdown increased p62, PKG, Bcl-2 and eNOS expression, while decreasing Beclin-1, caspase-9, caspase-3, LC3-II/LC3-I, Bax, VCAM-1 and ICAM-1 levels (Fig. 4B). These results suggested that circRNA_013145 silencing alleviated HG-induced phenotypic transformation, apoptosis, autophagy-associated activation and endothelial inflammatory injury *in vitro*.

circRNA_013145 serves as an miRNA sponge for miR-185-5p. Given the predominant cytoplasmic localization of circRNA_013145, it was hypothesized its involvement in the biological activity of CCSMCs and HUVECs may be mediated via miRNA sponge interactions. miR-185-5p was identified as a candidate with a binding site within the circRNA_013145 sequence (Fig. 5A). Luciferase assay confirmed that increased levels of miR-185-5p notably decreased luciferase activity in CCSMCs and HUVECs within the circ-WT group, but had no effect on luciferase activity in CCSMCs and HUVECs in the circ-Mut group (Fig. 5B).

The present study demonstrated a significant decrease in miR-185-5p expression levels in penile tissue (Fig. 5C) and HG-induced CCSMCs and HUVECs (Fig. 5D). RT-qPCR analysis confirmed that miR-185-5p mimic markedly increased miR-185-5p levels, whereas the miR-185-5p inhibitor significantly decreased miR-185-5p levels in CCSMCs and HUVECs (Fig. 5E). In addition, circRNA_013145 expression was negatively associated with miR-185-5p expression in CCSMCs and HUVECs (Fig. 5F), with circRNA_013145 knockdown significantly increasing miR-185-5p expression (Fig. 5G). These findings suggested that circRNA_013145 interacts with miR-185-5p during DMED development.

circRNA_013145 may regulate RhoA expression by sponging miR-185-5p. Bioinformatics analyses revealed RhoA as a target gene for miR-185-5p (Fig. 6A). Luciferase assay confirmed that miR-185-5p binds to RhoA 3'-UTR, leading to decreased RhoA luciferase activity in CCSMCs and HUVECs (Fig. 6B).

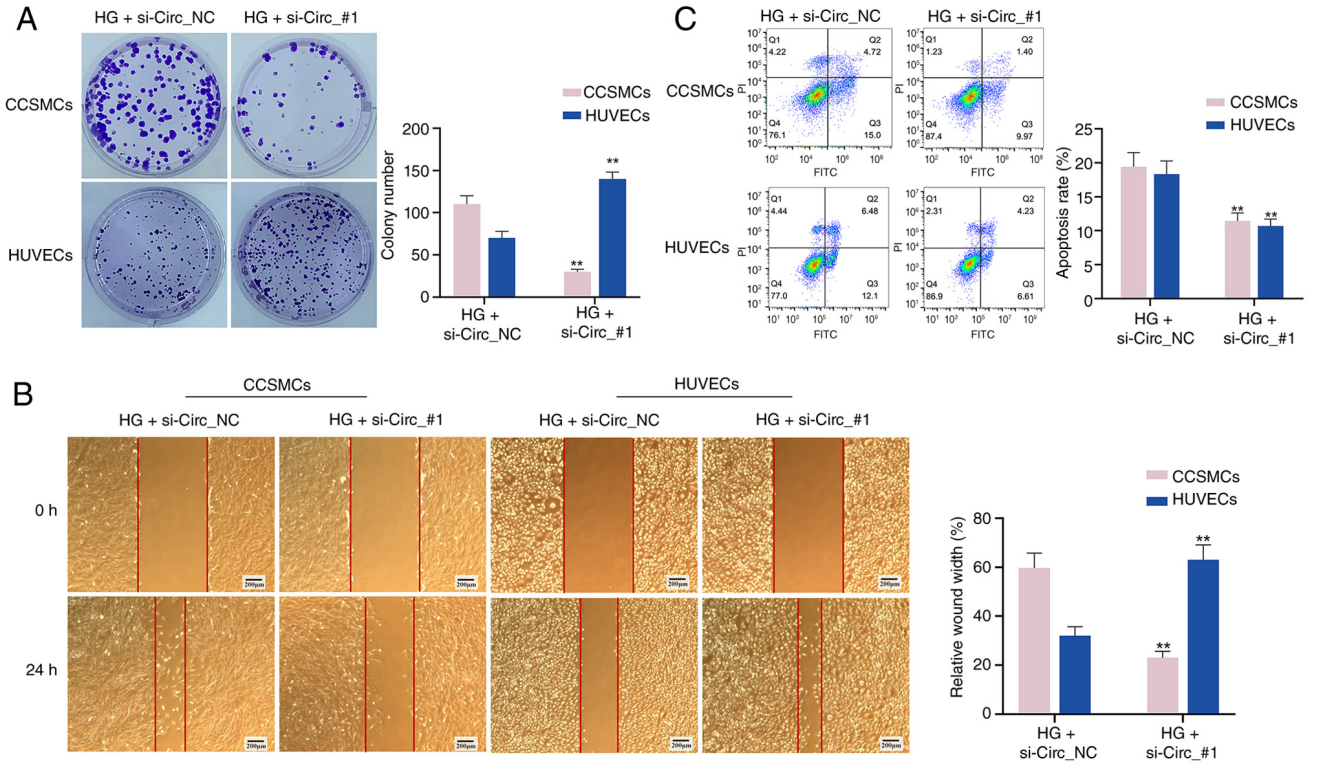

Figure 3. Effects of circRNA_013145 knockdown on CCSMC and HUVEC proliferation, migration and apoptosis. (A) Effect of circRNA_013145 knockdown on cell proliferation was determined via the colony formation assay. (B) Effect of circRNA_013145 knockdown on migration was determined via the wound-healing assay. (C) Apoptosis levels in transfected CCSMCs and HUVECs, as determined via flow cytometry. **P<0.01 vs. si-circ_NC. circ, circular; CCSMC, corpus cavernosum smooth muscle cell; HUVEC, human umbilical vein endothelial cell; si, small interfering; NC, negative control; HG, high-glucose.

RhoA expression was significantly higher in penile tissue from DMED rats than in control rats (Fig. 6C) and in HG-induced CCSMCs and HUVECs compared with the corresponding control cells (Fig. 6D).

The connection between RhoA, miR-185-5p and circRNA_013145 was verified by RIP assays with anti-Ago2 antibodies. circRNA_013145, miR-185-5p and RhoA levels were significantly higher in CCSMCs and HUVECs in the Ago2 group than in CCSMCs and HUVECs in the IgG groups (Fig. 6E). Transfection with miR-185-5p mimic significantly inhibited RhoA expression in CCSMCs and HUVECs (Fig. 6F). Similarly, circRNA_013145 knockdown with si-Circ_#1 decreased RhoA protein levels in both cell types (Fig. 6G). Collectively, these findings demonstrated that the circRNA_013145/miR-185-5p/RhoA pathway may contribute to DMED progression.

miR-185-5p downregulation reverses the effects of circRNA_013145knockdown. To determine whether miR-185-5p mediates the protective effects of circRNA_013145 knockdown, rescue experiments were performed by co-transfecting si-Circ#1 with a miR-185-5p inhibitor under HG conditions. In the colony formation assay, si-Circ#1 decreased CCSMC but enhanced HUVEC proliferation, whereas miR-185-5p inhibition partially reversed these effects (Fig. 7A). Flow cytometry showed that circRNA_013145 knockdown decreased apoptosis in both CCSMCs and HUVECs and this anti-apoptotic effect was weakened by miR-185-5p inhibition (Fig. 7B). In the wound healing assay, si-Circ#1 suppressed CCSMC migration and promoted HUVEC migration, while co-transfection with the miR-185-5p inhibitor partially reversed these changes (Fig. 7C). si-Circ#1 decreased TNF-α, IL-6 and MDA and increased SOD, NO and cGMP levels, whereas miR-185-5p inhibition attenuated these improvements in inflammatory and oxidative stress-associated indicators (Fig. 7D). Consistently, western blotting showed that the si-circ#1-induced changes in phenotypic transformation-, apoptosis-, autophagy- and endothelial function-related proteins were also partially reversed by miR-185-5p inhibition (Fig. 7E). These findings indicated that circRNA_013145 aggravated HG-induced CCSMC and HUVEC injury, at least in part, via the miR-185-5p/RhoA regulatory pathway.

Effects of circRNA_013145 knockdown on erectile function, phenotypic transformation and apoptosis in rats with DMED. To evaluate the *in vivo* effects of circRNA_013145 knockdown, Ad-sh_circRNA_013145 was delivered into the CC of DMED rats. Behavioral assessment showed that DMED rats exhibited decreased erection frequency and duration, together with prolonged erection latency, whereas Ad-sh_circRNA_013145 partially restored these parameters compared with the DMED and Ad-NC groups (Fig. 8A). Consistently, max ICP and ICP/MAP ratio were markedly decreased in DMED rats and partially recovered following Ad-sh_circRNA_013145 treatment (Fig. 8B).

Histological analysis showed marked cavernosal remodeling in DMED rats. H&E staining revealed a decrease in the number of visible blood vessels and vascular-like structures in the CC, whereas Masson's trichrome staining showed increased collagen deposition and decreased smooth muscle

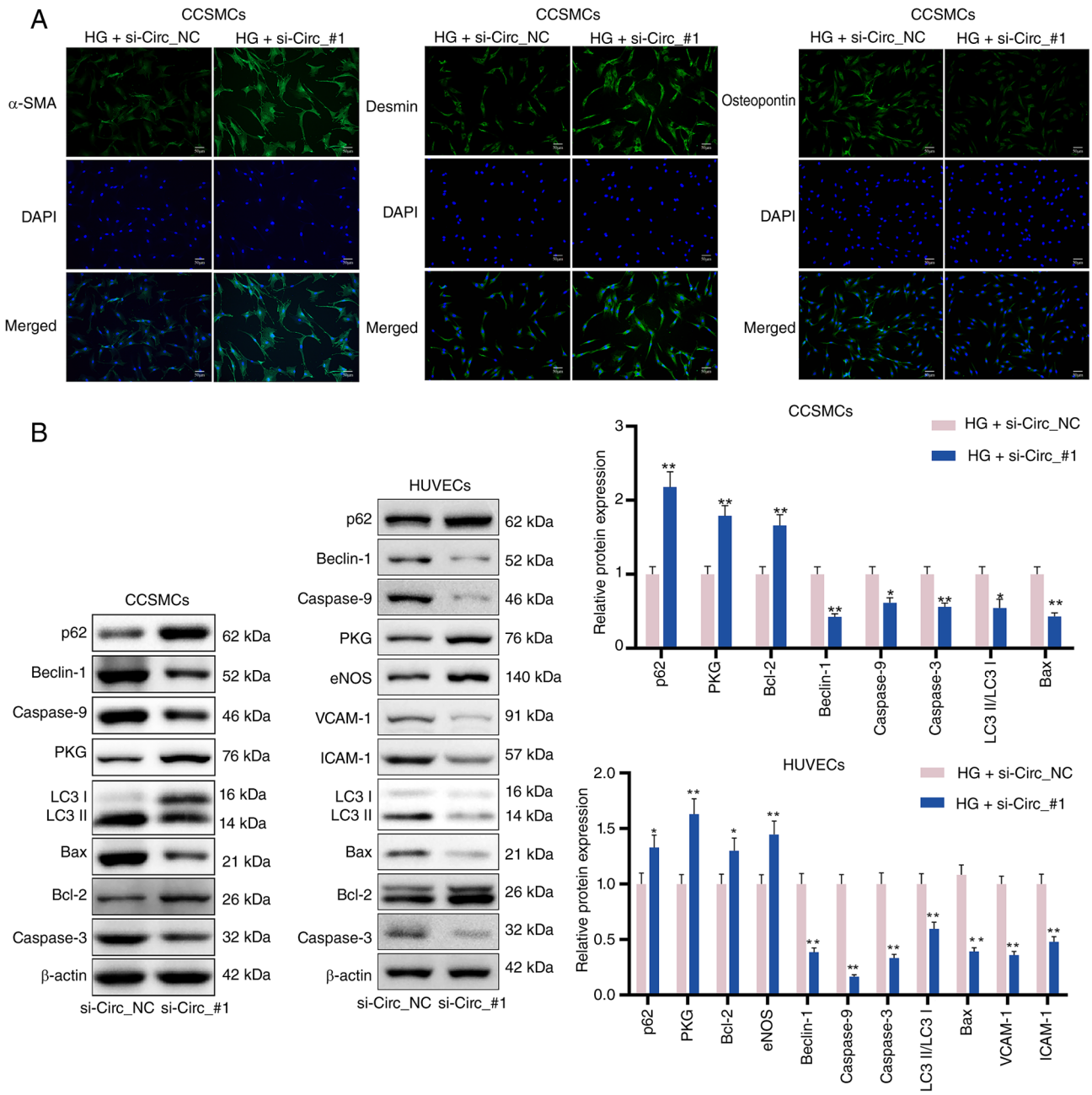

Figure 4. Effects of circRNA_013145 knockdown on phenotypic transformation and apoptosis-associated protein expression levels in CCSMCs and HUVECs. (A) α-SMA, desmin and osteopontin protein expression levels analyzed using immunofluorescence staining. Scale bar, 50 μm. (B) p62, PKG, Bcl-2, Beclin-1, Caspase-9, LC3, Bax and Caspase-3 protein expression levels in CCSMCs and p62, PKG, Bcl-2, eNOS, Beclin-1, Caspase-9, Caspase-3, LC3, Bax, VCAM-1 and ICAM-1 protein expression levels in si-circRNA_013145-transfected HUVECs, as determined via western blotting. *P<0.05, **P<0.01 vs. HG + si-circ_NC. circ, circular; CCSMC, corpus cavernosum smooth muscle cell; HUVECs, human umbilical vein endothelial cell; α-SMA, α-smooth muscle actin; PKG, protein kinase G; eNOS, endothelial nitric oxide synthase; VCAM-1, vascular cell adhesion molecule-1; ICAM-1, intercellular adhesion molecule-1; LC3, microtubule-associated protein 1 light chain 3; HG, high-glucose; si, small interfering; NC, negative control.

content. These pathological changes were partially reversed by Ad-sh_circRNA_013145 (Fig. 8C). CD31 immunofluorescence staining also showed that CD31-positive vascular structures were decreased in the DMED and Ad-NC groups, whereas Ad-sh_circRNA_013145 increased the number of CD31-positive vascular structures in the CC (Fig. 8D). TUNEL staining demonstrated increased apoptosis in DMED penile tissue, which was significantly decreased following Ad-sh_circRNA_013145 treatment (Fig. 8E).

The *in vivo* knockdown efficiency of Ad-sh_circRNA_013145 was validated by RT-PCR. Compared with Ad-sh_NC, Ad-sh_circRNA_013145 significantly decreased circRNA_013145 expression in rat penile tissue (Fig. S7C). RT-qPCR showed that Ad-sh_circRNA_013145 increased miR-185-5p expression and decreased RhoA expression in DMED penile tissue (Fig. 8F). Western blotting showed that Ad-sh_circRNA_013145 increased α-SMA, desmin, p62, PKG, eNOS and Bcl-2 levels, while decreasing RhoA, Beclin-1, VCAM-1, ICAM-1, osteopontin, LC3-II/LC3-I and Bax levels (Fig. 8G). These *in vivo* findings were consistent with the *in vitro* results and suggested that circRNA_013145 knockdown improves erectile

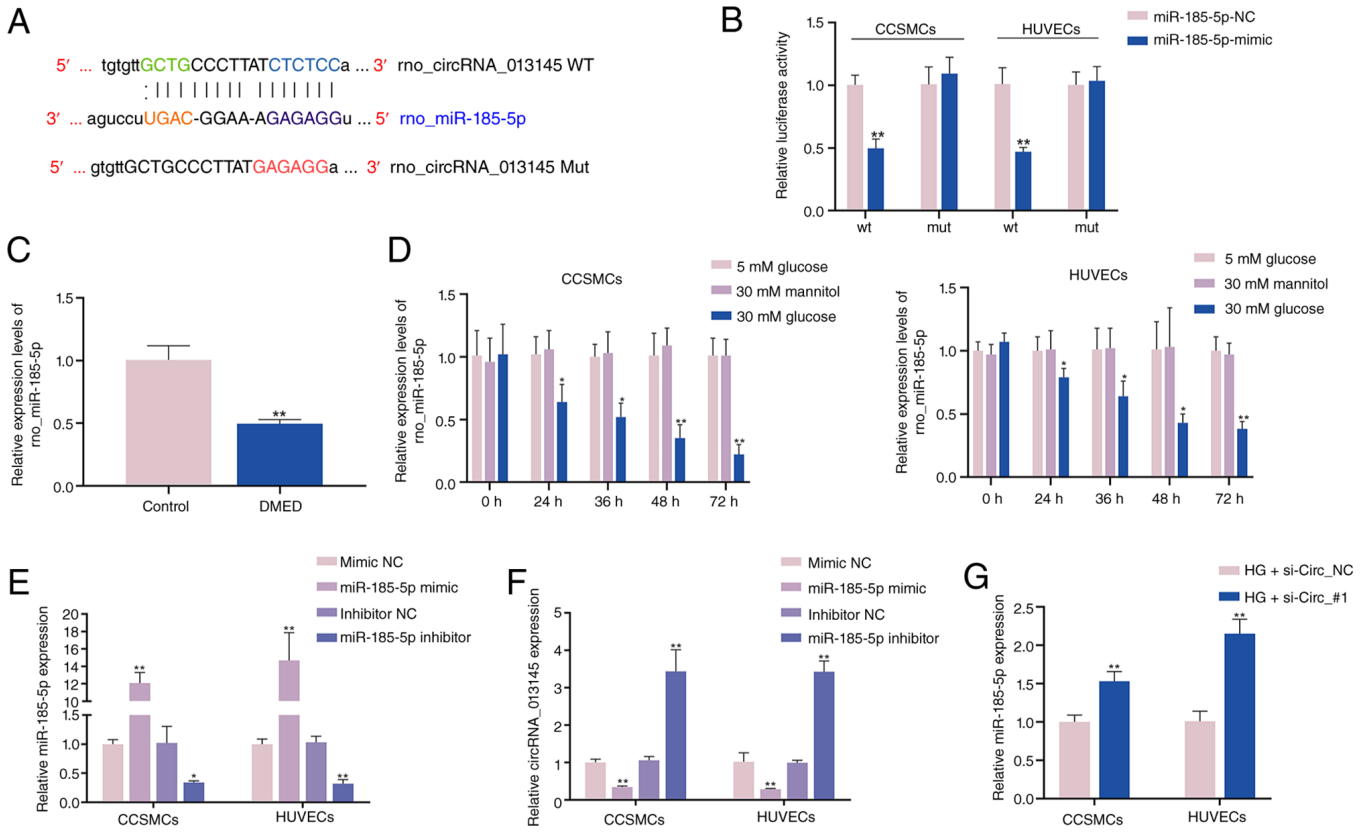

Figure 5. circRNA_013145 acts as a sponge for miR-185-5p in CCSMCs and HUVECs. (A) Potential binding sites for circRNA_013145 and miR-185-5p. (B) Direct interaction between circRNA_013145 and miR-185-5p in CCSMCs and HUVECs was determined via a luciferase reporter assay. miR-185-5p expression in (C) penile tissue and (D) HG-induced CCSMCs and HUVECs as determined via quantitative PCR. (E) miR-185-5p levels in CCSMCs and HUVECs transfected with miR-185-5p mimics or the miR-185-5p inhibitor. (F) circRNA_013145 expression levels in CCSMCs and HUVECs transfected with miR-185-5p mimic or miR-185-5p inhibitor. (G) miR-185-5p expression in HG-induced CCSMCs and HUVECs transfected with circRNA_013145 siRNA. *P<0.05, **P<0.01 vs. miR-NC, control, vector NC or si-circ_NC in F and vs. HG + si-circ_NC. circ, circular; miR, microRNA; CCSMC, corpus cavernosum smooth muscle cells; HUVECs, human umbilical vein endothelial cell; si, small interfering; WT, wild-type; Mut, mutant; NC, negative control; HG, high-glucose.

function and cavernosal pathological remodeling through the miR-185-5p/RhoA-associated pathway.

Discussion

DMED is a common and difficult to treat complication of diabetes, and its pathogenesis involves complex interactions between endothelial dysfunction, oxidative stress, inflammation, cavernosal smooth muscle injury and structural remodeling (1,30). Hyperglycemia-induced oxidative stress and inflammatory responses are key contributors to endothelial damage (31), whereas phenotypic transformation of CCSMCs compromises cavernosal relaxation and penile hemodynamics (32,33). The present study identified circRNA_013145 as a significantly upregulated circRNA in penile tissue from DMED rats and in HG-treated CCSMCs and HUVECs. These findings suggested that circRNA_013145 may participate in the pathological response of cavernosal vascular and smooth muscle cells to diabetic conditions.

A key step in circRNA research is distinguishing the circular transcript from its corresponding linear host transcript. circRNA_013145 is derived from the Asph gene; the present RNase R and actinomycin D assay demonstrated that circRNA_013145 was more stable than linear Asph mRNA and resistant to RNase R digestion, supporting its identity as a circRNA. In addition, nuclear-cytoplasmic fractionation and FISH analysis showed that circRNA_013145 was predominantly localized in the cytoplasm, indicating that it may exert post-transcriptional regulatory effects. Consistent with this, dual-luciferase reporter assay and RIP analysis confirmed that circRNA_013145 directly interacted with miR-185-5p. Moreover, luciferase reporter assays supported the binding of miR-185-5p to the RhoA 3'-UTR), and circRNA_013145 knockdown reduced RhoA expression in a miR-185-5p-dependent manner. These data identified circRNA_013145/miR-185-5p/RhoA as a key regulatory pathway in DMED. A schematic summary of the proposed circRNA_013145/miR-185-5p/RhoA regulatory mechanism in DMED is shown in Fig. S8.

The decline in erectile function in DMED is associated with cavernosal vascular dysfunction, impaired neurovascular repair, smooth muscle loss, collagen deposition and fibrosis (34-36). These pathological changes compromise penile blood filling, veno-occlusive function and erectile hemodynamics. In the present study, circRNA_013145 knockdown partially restored erectile behavior, increased max ICP and the ICP/MAP ratio, increased the number of CD31-positive vascular structures and decreased cavernosal fibrosis and apoptosis in DMED rats. At the cell level, circRNA_013145 knockdown attenuated HG-induced oxidative stress and inflammation, restored NO/cGMP- and PKG-associated

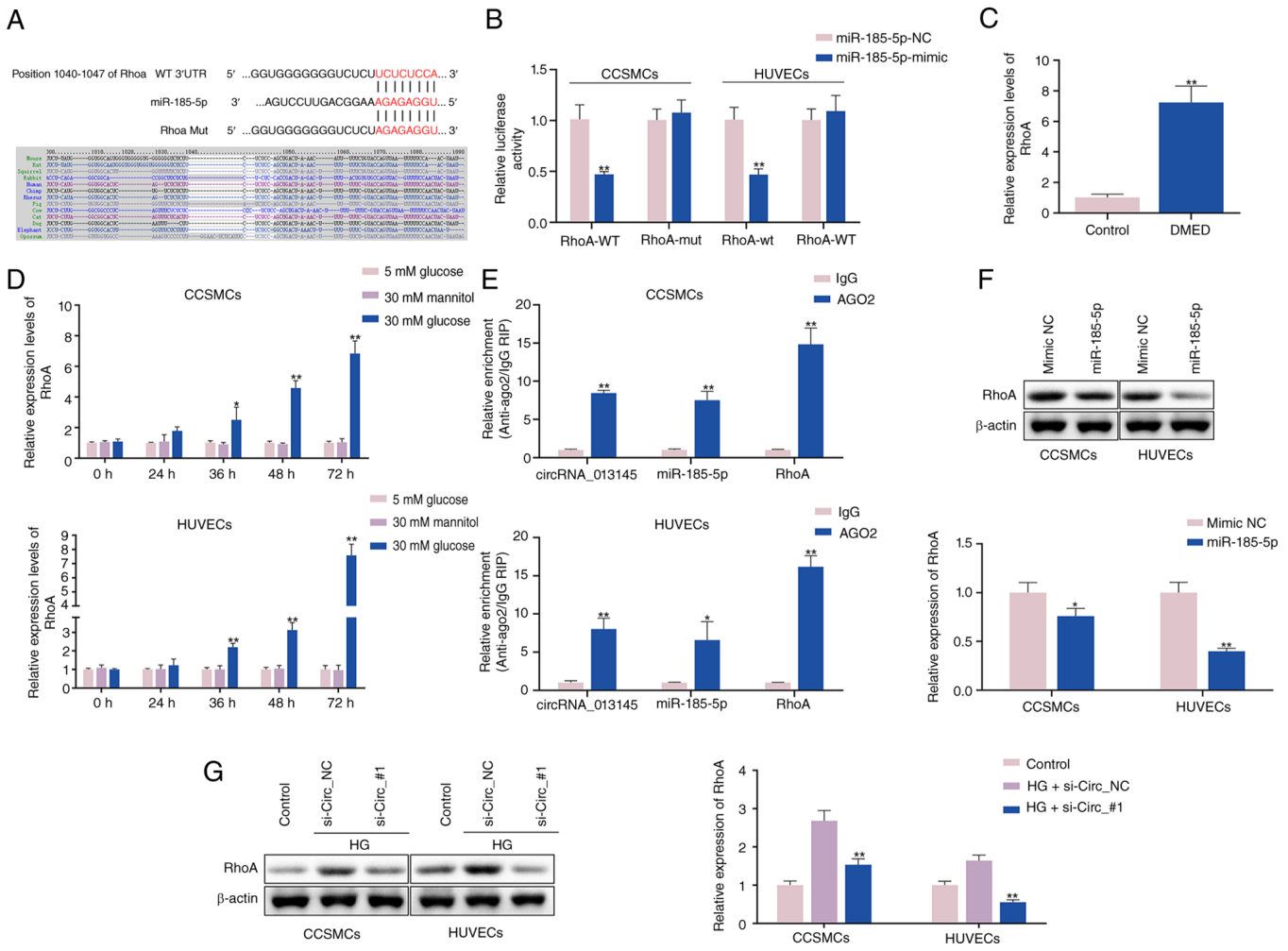

Figure 6. miR-185-5p targets the 3'-UTR of RhoA. (A) Predicted binding site for miR-185-5p within the RhoA 3'-UTR. (B) Interaction between miR-185-5p and RhoA as determined via a luciferase reporter assay. RhoA expression in (C) penile tissues of rats with diabetes mellitus erectile dysfunction and (D) HG-induced CCSMCs and HUVECs. (E) Enrichment of circRNA_013145, miR-185-5p and RhoA on Ago2, relative to IgG, as determined via RIP assay. (F) RhoA protein expression levels in CCSMCs and HUVECs transfected with miR-185-5p mimic, as determined using western blotting. (G) RhoA protein expression levels in HG-treated CCSMCs and HUVECs transfected with si-circRNA_013145, as determined using western blotting. *P<0.05, **P<0.01 vs. miR-NC, control in C, vs. 5 mM glucose in D, vs. IgG in E and vs. HG + si-circ_NC in G. miR, microRNA; UTR, untranslated region; HG, high-glucose; CCSMC, corpus cavernosum smooth muscle cells; HUVECs, human umbilical vein endothelial cells; circ, circular; RIP, RNA immunoprecipitation; Ago2, Argonaute 2; si, small interfering; NC, negative control; WT, wild-type; Mut, mutant.

indicators and improved the biological behavior of CCSMCs and HUVECs. Given the key role of the NO/cGMP/PKG pathway in erectile physiology (19,37), these results suggested that circRNA_013145 may contribute to DMED by linking hyperglycemia-induced cell injury with impaired cavernosal vascular function. Oxidative stress is also a key mechanism that disrupts endothelial function, decreases NO bioavailability and contributes to ED (38).

circRNAs typically regulate gene expression by acting as miRNA sponges, interacting with RNA-binding proteins or modulating post-transcriptional processes (39). Increasing evidence also indicates that circRNAs participate in diabetes and its vascular complications (16,40). In the present study, circRNA_013145 was primarily localized in the cytoplasm of CCSMCs and HUVECs, supporting a potential post-transcriptional regulatory role. The present study identified circRNA_013145 as a sponge for miR-185-5p and confirmed RhoA as a downstream target of miR-185-5p. Advanced glycation end products disrupt endothelial function through RhoA-related signaling (41). RhoA/ROCK activation may negatively influence NO/cGMP-mediated relaxation, which is key for normal erectile function (42). More broadly, RhoA/ROCK signaling contributes to endothelial dysfunction, vascular smooth muscle remodeling and diabetes-associated vascular injury (43,44), and pharmacological inhibition of this pathway has been shown to improve ED in preclinical models (45,46). Therefore, the circRNA_013145/miR-185-5p/RhoA pathway may represent a mechanistic link between hyperglycemia-induced non-coding RNA dysregulation and cavernosal vascular dysfunction in DMED.

Functionally, circRNA_013145 silencing attenuated multiple pathological processes associated with DMED. In CCSMCs, circRNA_013145 knockdown increased levels of the contractile markers α-SMA and desmin and decreased expression of the synthetic marker osteopontin, suggesting inhibition of HG-induced phenotypic transformation. In HUVECs, circRNA_013145 knockdown increased eNOS expression and decreased VCAM-1 and ICAM-1 levels, indicating

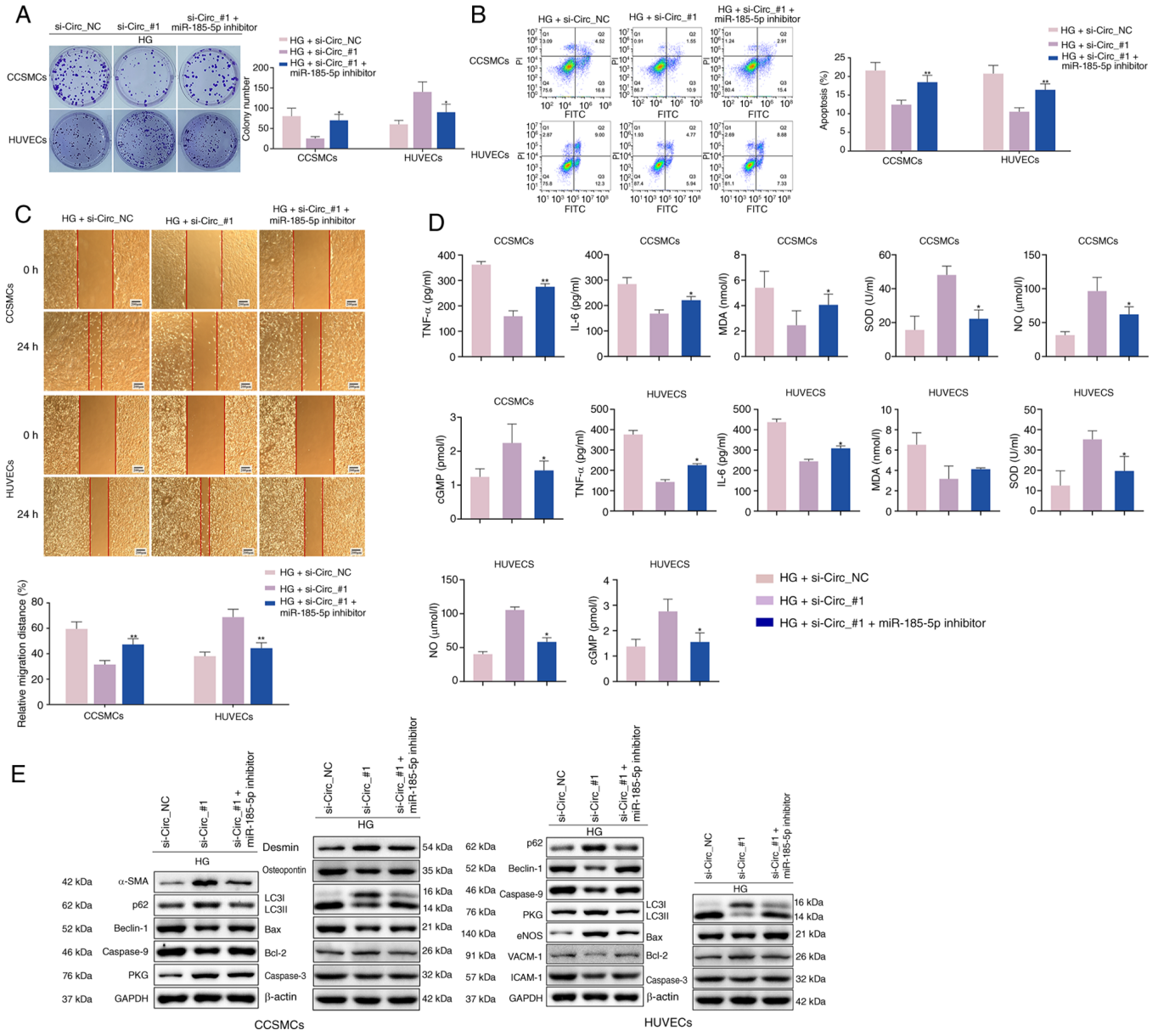

Figure 7. miR-185-5p inhibition reverses the protective effects of circRNA_013145 knockdown. (A) Co-transfected CCSMC and HUVEC proliferation as determined via a colony formation assay. (B) Representative flow cytometric images showing the effects of miR-185-5p in CCSMCs and HUVECs on circRNA_013145 silencing. (C) Migration of co-transfected CCSMCs and HUVECs as determined via a wound healing assay. (D) TNF-α, IL-6, MDA, SOD, NO and cGMP levels in co-transfected CCSMCs and HUVECs, as determined via ELISA. (E) miR-185-5p knockdown abolished the effects of si-circRNA_013145 on α-SMA, desmin, osteopontin, p62, LC3, Beclin-1, Bax, Bcl-2, Caspase-9, Caspase-3, PKG, eNOS, VCAM-1 and ICAM-1 expression in HG-induced CCSMCs and HUVECs. *P<0.05, **P<0.01 vs. HG + si-Circ_#1. miR, microRNA; circ, circular; CCSMC, corpus cavernosum smooth muscle cells; HUVECs, human umbilical vein endothelial cells; MDA, malondialdehyde; SOD, superoxide dismutase; NO, nitric oxide; cGMP, cyclic guanosine monophosphate; α-SMA, α-smooth muscle actin; PKG, protein kinase G; eNOS, endothelial nitric oxide synthase; VCAM-1, vascular cell adhesion molecule-1; ICAM-1, intercellular adhesion molecule-1; HG, high-glucose; NC, negative control.

improvement of endothelial inflammatory injury. In both cell types, circRNA_013145 silencing decreased expression of apoptosis- and autophagy-associated injury markers, including Bax, caspase-3/9, Beclin-1 and LC3-II/LC3-I, while increasing Bcl-2 and p62. Autophagy has recently been recognized as a key regulator of erectile function under pathological conditions, including diabetes-associated injury (47). Although the present improvements are consistent with enhanced cell homeostasis after circRNA_013145 silencing, whether these changes are direct consequences of RhoA downregulation or involve additional downstream pathways remains to be clarified.

The rescue experiments supported the functional relevance of miR-185-5p in the regulatory axis. Inhibition of miR-185-5p partially reversed the beneficial effects of circRNA_013145 knockdown on proliferation, migration, apoptosis, inflammation, oxidative stress and protein markers related to CCSMC phenotype and endothelial function. These findings indicated that miR-185-5p is required, at least in part, for the protective effects induced by circRNA_013145 silencing. However, because circRNAs may interact with multiple miRNAs or RNA-binding proteins, additional targets of circRNA_013145 cannot be excluded.

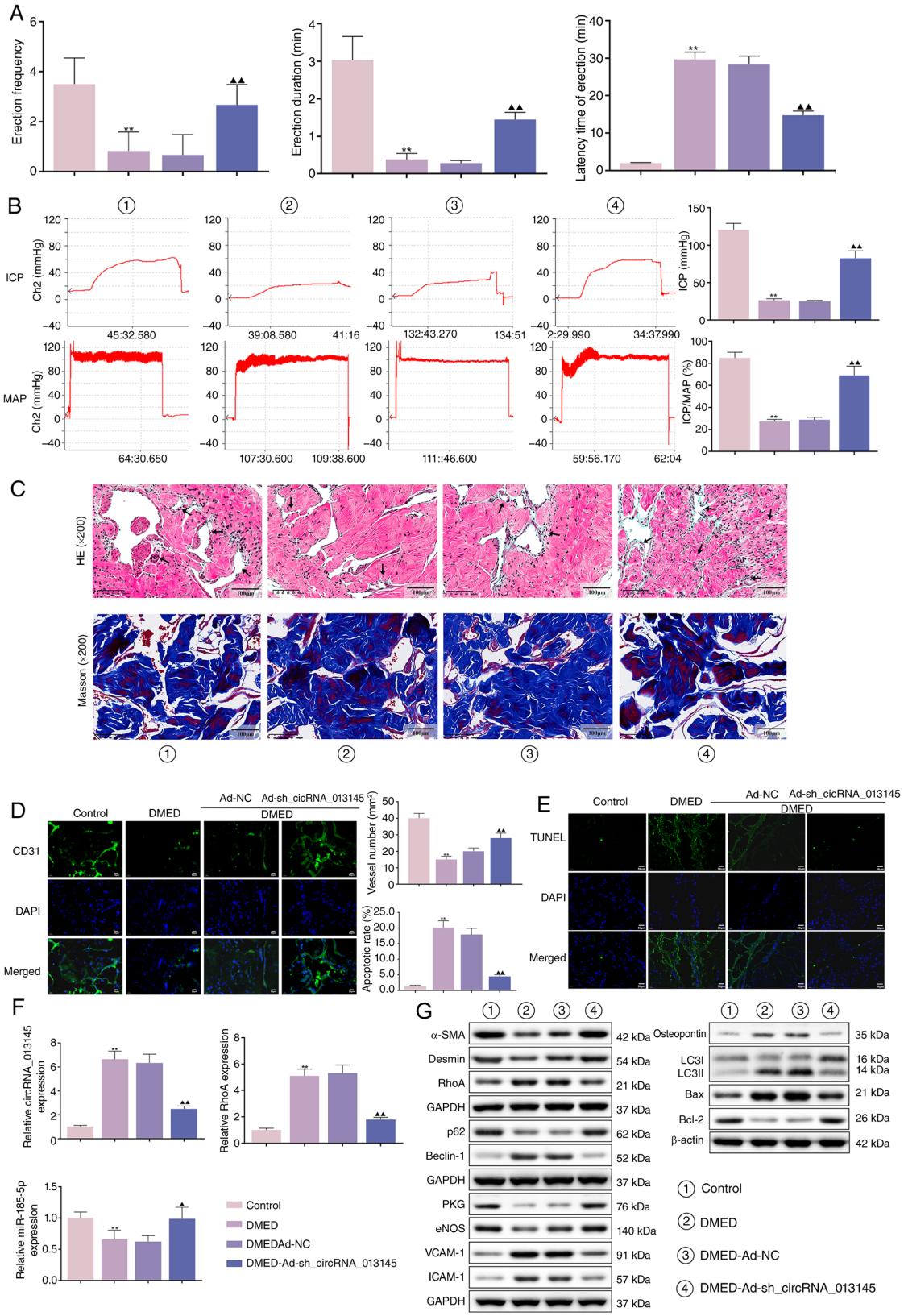

Figure 8. Effects of circRNA_013145 knockdown on erectile function, phenotypic transformation, and apoptosis in rats with DMED. (A) Assessment of erectile function, including erection duration, in Ad-sh_circRNA_013145-treated rats with DMED. (B) Representative traces of ICP and MAP in rats. (C) Representative H&E and Masson's staining (scale bar, 100 μm) of rat CC; arrows indicate blood vessels. Scale bar, 100 μm. (D) Representative CD31 immunofluorescence staining in rats with DMED. (E) Representative TUNEL staining of apoptotic cells in rat CC following sh_circRNA_013145 treatment. Scale bar, 100 μm. (F) circRNA_013145, miR-185-5p, and RhoA expression determined via reverse transcription-quantitative PCR. (G) Representative western blots for α-SMA, desmin, RhoA, p62, Beclin-1, PKG, eNOS, VCAM-1, ICAM-1, osteopontin, LC3, Bax and Bcl-2 expression in the penile tissue of rats. GAPDH or β-actin was used as the loading control. **P<0.01 vs. control; $^{▲}$P<0.05, $^{▲▲}$P<0.01 vs. DMED or DMED-Ad-NC. circ, circular; DMED, diabetes mellitus-induced erectile dysfunction; Ad, adenovirus; sh, short hairpin; ICP, intracavernosal pressure; MAP, mean arterial pressure; H&E, hematoxylin and eosin; CC, corpus cavernosum; miR, microRNA; α-SMA, α-smooth muscle actin; PKG, protein kinase G; eNOS, endothelial nitric oxide synthase; VCAM-1, vascular cell adhesion molecule-1; ICAM-1, intercellular adhesion molecule-1; NC, negative control.

The *in vivo* findings were consistent with the cellular results. At the molecular level, Ad-sh_circRNA_013145 decreased circRNA_013145 and RhoA expression while increasing miR-185-5p expression in penile tissue. Western blotting further confirmed favorable changes in markers of smooth muscle phenotype, endothelial function, apoptosis and autophagy-related activation. These results suggested that circRNA_013145 knockdown can improve both functional and structural abnormality in DMED, supporting the translational relevance of the circRNA_013145/miR-185-5p/RhoA pathway.

The present study has limitations. First, the use of a rat DMED model and *in vitro* cell systems limits direct extrapolation to human DMED. Second, although HUVECs provide a useful endothelial model, they do not fully recapitulate penile cavernous endothelial cells. Third, although the circRNA_013145/miR-185-5p/RhoA pathway was experimentally validated, other potential miRNA targets or RNA-binding protein interactions of circRNA_013145 were not explored. Fourth, the downstream involvement of RhoA/ROCK signaling, autophagy and apoptosis was primarily inferred from changes in associated markers; pathway-specific rescue or inhibition experiments are needed for stronger causal validation. Finally, the long-term efficacy and safety of Ad-mediated circRNA_013145 silencing remain to be investigated.

In conclusion, the present study demonstrated that circRNA_013145 was upregulated in DMED and promoted cavernosal cellular injury by sponging miR-185-5p and increasing RhoA expression. Silencing circRNA_013145 alleviated oxidative stress, inflammation, CCSMC phenotypic transformation, endothelial injury, apoptosis and cavernosal remodeling, improving erectile function in DMED rats. These findings identified circRNA_013145 as a potential molecular target for DMED and provide new insight into circRNA-mediated regulation of diabetic cavernosal dysfunction.

Acknowledgements

Not applicable.

Funding

The present study was supported by Scientific Research Project Talent Program of Zhejiang Chinese Medical University (grant no. 2023RCZXZK47).

Availability of data and materials

The data generated in the present study may be found in the Gene Expression Omnibus under accession number GSE328657 or at the following URL: ncbi.nlm.nih.gov/geo/query/acc.cgi?acc=GSE328657.

Authors' contributions

WH designed the experiments, constructed figures and wrote the manuscript. XL, JQ and YC designed the experiments and constructed figures. YS and JW designed the experiments. JM conceived the study and edited the manuscript. WH and JM confirm the authenticity of all the raw data. All authors have read and approved the final manuscript.

Ethics approval and consent to participate

Animal research was approved by the Animal Care and Use Committee of Zhejiang Chinese Medical University, Hangzhou, China (approval no. ZSLL-2021-164).

Patient consent for publication

Not applicable.

Competing interests

The authors declare that they have no competing interests.

References

1. Hostnik B, Tonin G, Janež A and Klen J: Erectile dysfunction in diabetes mellitus: A comprehensive narrative review of pathophysiology, genetic association studies and therapeutic approaches. Endocrinol Diabetes Metab 8: e70099, 2025.
2. Yu XD, Wang JS, Zuo G, Wang X, Ge F, Wu S, Lim J, Shang J and Zhang Y: Traditional Chinese medicine on treating diabetic mellitus erectile dysfunction: Protocol for a systematic review and meta-analysis. Medicine (Baltimore) 98: e14928, 2019.
3. Zhang X, Yang B, Li N and Li H: Prevalence and risk factors for erectile dysfunction in Chinese adult males. J Sex Med 14: 1201-1208, 2017.
4. Yang B, Cheng H, Hu Y, Chen Y, Xu Y, Huang W, Long Y and Gao C: Effects of Anti-diabetic drugs on erectile dysfunction: A systematic review and meta-analysis. Diabetes Metab Syndr Obes 18: 467-478, 2025.
5. Begum M, Choubey M, Tirumalasetty MB, Arbee S, Sadik S, Mohib MM, Srivastava S, Minhaz N, Alam R and Mohiuddin MS: Exploring the molecular link between diabetes and erectile dysfunction through single-cell transcriptome analysis. Genes (Basel) 15: 1596, 2024.
6. Cheng J, Liu Q, Hu N, Zheng F, Zhang X, Ni Y and Liu J: Downregulation of hsa_circ_0068087 ameliorates TLR4/NF-κB/NLRP3 inflammasome-mediated inflammation and endothelial cell dysfunction in high glucose conditioned by sponging miR-197. Gene 709: 1-7, 2019.
7. Bozkurt YE, Gümüş BH, Düzgün F and Neşe N: Comparison of preoperative penile elastographic ultrasound findings and pathological tissue results of patients implemented with penile prosthesis. J Ultrasound 26: 99-105, 2023.
8. Zhou X, Luo C, Fan J, Gao G, Wang T, Zhang H and Wei A: Myocardin reverses hypoxia-inducible factor-1α mediated phenotypic modulation of corpus cavernosum smooth muscle cells in hypoxia induced by cobalt chloride. World J Mens Health 41: 363-372, 2023.
9. Chen S, Huang X, Kong X, Sun Z, Zhao F, Huang W, Ye M, Ma K, Tao T and Lv B: Hypoxia-induced phenotypic transformation of corpus cavernosum smooth muscle cells after cavernous nerve crush injury by down-regulating P38 mitogen-activated protein kinase expression. Sex Med 7: 433-440, 2019.
10. Zeng Q, He S, Chen F, Wang L, Zhong L, Hui J, Ding W, Fan J, Zhang H and Wei A: Administration of H_2S improves erectile dysfunction by inhibiting phenotypic modulation of corpus cavernosum smooth muscle in bilateral cavernous nerve injury rats. Nitric Oxide 107: 1-10, 2021.
11. He S, Zhang T, Liu Y, Liu L, Zhang H, Chen F and Wei A: Myocardin restores erectile function in diabetic rats: Phenotypic modulation of corpus cavernosum smooth muscle cells. Andrologia 47: 303-309, 2015.
12. Patop IL, Wüst S and Kadener S: Past, present, and future of circRNAs. EMBO J 38: e100836, 2019.
13. Foruzandeh Z, Zeinali-Sehrig F, Nejati K, Rahmanpour D, Pashazadeh F, Seif F and Alivand MR: CircRNAs as potent biomarkers in ovarian cancer: A systematic scoping review. Cell Mol Biol Lett 26: 41, 2021.
14. Kristensen LS, Andersen MS, Stagsted LVW, Ebbesen KK, Hansen TB and Kjems J: The biogenesis, biology and characterization of circular RNAs. Nat Rev Genet 20: 675-691, 2019.

15. Shi X, Liao S, Bi Z, Liu J, Li H and Feng C: Newly discovered circRNAs encoding proteins: Recent progress. Front Genet 14: 1264606, 2023.
16. Dieter C, Girardi E, Vieira IA, Kowalski TW, Giudicelli GC, Lemos NE and Crispim D: Circular RNAs in diabetes mellitus and its complications: A systematic review and in silico analyses. Endocr Connect 14: e250484, 2025.
17. Xie Q, Ma Y, Ren Z, Gu T and Jiang Z: Circular RNA: A new expectation for cardiovascular diseases. J Cell Biochem 125: e30512, 2024.
18. Conn VM, Chinnaiyan AM and Conn SJ: Circular RNA in cancer. Nat Rev Cancer 24: 597-613, 2024.
19. Ma JX, Wang B, Li HS, Yu J, Hu HM, Ding CF and Chen WQ: Uncovering the mechanisms of leech and centipede granules in the treatment of diabetes mellitus-induced erectile dysfunction utilising network pharmacology. J Ethnopharmacol 265: 113358, 2021.
20. American Veterinary Medical Association: AVMA Guidelines for the Euthanasia of Animals: 2020 edition. American Veterinary Medical Association. Schaumburg, IL, 2020. https://www.avma.org/sites/default/files/2020-02/Guidelines-on-Euthanasia-2020.pdf.
21. Agarwal V, Bell GW, Nam JW and Bartel DP: Predicting effective microRNA target sites in mammalian mRNAs. Elife 4: e05005, 2015.
22. Enright AJ, John B, Gaul U, Tuschl T, Sander C and Marks DS: MicroRNA targets in Drosophila. Genome Biol 5: R1, 2003.
23. Sticht C, De La Torre C, Parveen A and Gretz N: miRWalk: An online resource for prediction of microRNA binding sites. PLoS One 13: e0206239, 2018.
24. Zhou Y, Zhou B, Pache L, Chang M, Khodabakhshi AH, Tanaseichuk O, Benner C and Chanda SK: Metascape provides a biologist-oriented resource for the analysis of systems-level datasets. Nat Commun 10: 1523, 2019.
25. Szklarczyk D, Gable AL, Lyon D, Junge A, Wyder S, Huerta-Cepas J, Simonovic M, Doncheva NT, Morris JH, Bork P, *et al*: STRING v11: Protein-protein association networks with increased coverage, supporting functional discovery in genome-wide experimental datasets. Nucleic Acids Res 47 (D1): D607-D613, 2019.
26. Chung H, Jung SH, Ryu JK, Kim B, Kim HS and Yang SK: Isolation and characterization of smooth muscle cells from rat corpus cavernosum tissue for the study of erectile dysfunction. Korean J Urol 53: 556-563, 2012.
27. Arocho A, Chen B, Ladanyi M and Pan Q: Validation of the 2-DeltaDeltaCt calculation as an alternate method of data analysis for quantitative PCR of BCR-ABL P210 transcripts. Diagn Mol Pathol 15: 56-61, 2006.
28. Niu Z, Ren G, Huang L and Mu L: Circ_0008529 contributes to renal tubular cell dysfunction in high glucose stress via miR-185-5p/SMAD2 pathway in diabetic nephropathy. Biochem Genet 61: 963-978, 2023.
29. Wang T, Li N, Yuan L, Zhao M, Li G, Chen Y and Zhou H: MALAT1/miR-185-5p mediated high glucose-induced oxidative stress, mitochondrial injury and cardiomyocyte apoptosis via the RhoA/ROCK pathway. J Cell Mol Med 27: 2495-2506, 2023.
30. Ma J, Chen Y, Si Y, Qian J, Wang C, Jin J and He Q: The multifaceted nature of diabetic erectile dysfunction: Uncovering the intricate mechanisms and treatment strategies. Front Endocrinol (Lausanne) 15: 1460033, 2024.
31. Li X, Zou J, Lin A, Chi J, Hao H, Chen H and Liu Z: Oxidative stress, endothelial dysfunction, and N-acetylcysteine in type 2 diabetes mellitus. Antioxid Redox Signal 40: 968-989, 2024.
32. Ding W, Fan JH, Zhong LR, Wang NX, Liu LH, Zhang HB, Wang L, Wang MQ, He BL and Wei AY: N-acetylcysteine ameliorates erectile dysfunction in rats with hyperlipidemia by inhibiting oxidative stress and corpus cavernosum smooth muscle cells phenotypic modulation. Asian J Androl 26: 99-106, 2024.
33. Bae SG, Yin GN, Ock J, Suh JK, Ryu JK and Park J: Single-cell transcriptome analysis of cavernous tissues reveals the key roles of pericytes in diabetic erectile dysfunction. Elife 12: RP88942, 2024.
34. Lin Y, Hui J, Pan M, Wang L, Luo J, Chen Z, Zhang H and Wei A: Inhibition of YAP1 rescues erectile dysfunction by inhibiting phenotypic modulation through myocardin in diabetic rats. Andrologia 2024: 9964228, 2024.
35. Kwon MH, Rho BY, Choi MJ, Limanjaya A, Ock J, Yin GN, Jin SW, Suh JK, Chung DY and Ryu JK: BMP2 restores erectile dysfunction through neurovascular regeneration and fibrosis reduction in diabetic mice. Andrology 12: 447-458, 2024.
36. Tu B, Liu K, Wen B, Hu P, Sun T, Li B, Sulaiman M, Jiang S, Wang T, Liu J and Luan Y: Relaxin-2 improves type I diabetes mellitus-induced erectile dysfunction in rats by protecting cavernous endothelial and smooth muscle function, and inhibiting penile fibrosis and apoptosis. Andrology 13: 1935-1946, 2025.
37. Samidurai A, Xi L, Das A and Kukreja RC: Beyond erectile dysfunction: cGMP-specific phosphodiesterase 5 inhibitors for other clinical disorders. Annu Rev Pharmacol Toxicol 63: 585-615, 2023.
38. Zhu D, Pham QM, Wang C, Colonnello E, Yannas D, Nguyen BH, Zhang Y, Jannini EA and Sansone A: Erectile dysfunction and oxidative stress: A narrative review. Int J Mol Sci 26: 3073, 2025.
39. Hwang HJ and Kim YK: 2024: Molecular mechanisms of circular RNA translation. Exp Mol Med 56: 1272-1280, 2024.
40. Yuan L, Duan J and Zhou H: Perspectives of circular RNAs in diabetic complications from biological markers to potential therapeutic targets (review). Mol Med Rep 28: 194, 2023.
41. Li X, Tao Y, Wang X, Wang T and Liu J: Advanced glycosylation end products (AGEs) controls proliferation, invasion and permeability through orchestrating ARHGAP18/RhoA pathway in human umbilical vein endothelial cells. Glycoconj J 37: 209-219, 2020.
42. Shamloul R and Ghanem H: Erectile dysfunction. Lancet 381: 153-165, 2013.
43. Nunes KP, Rigsby CS and Webb RC: RhoA/Rho-kinase and vascular diseases: What is the link? Cell Mol Life Sci 67: 3823-3836, 2010.
44. Sun L, Huang N, Yang C, Feng J, Chen H, Feng W, Gao Z, Wang B and Wang J: Hirudin-based treatment of diabetes-induced erectile dysfunction through inhibition of the HIF-1α to regulate RhoA/ROCK signaling pathway: An in vivo animal experiment. Am J Mens Health 19: 15579883241310763, 2025.
45. Mahmood J, Pandita R, Zhang A, Kamlapurkar S, Saeed A, Chen M, Staats PN, Shukla HD, Anvari A, Sawant A and Vujaskovic Z: RhoA/ROCK pathway inhibitor ameliorates erectile dysfunction induced by radiation therapy in rats. Radiother Oncol 150: 174-180, 2020.
46. Bivalacqua TJ, Champion HC, Usta MF, Cellek S, Chitaley K, Webb RC, Lewis RL, Mills TM, Hellstrom WJ and Kadowitz PJ: RhoA/Rho-kinase suppresses endothelial nitric oxide synthase in the penis: A mechanism for diabetes-associated erectile dysfunction. Proc Natl Acad Sci USA 101: 9121-9126, 2004.
47. Wu C, Xiong Y, Fu F, Zhang F, Qin F and Yuan J: The role of autophagy in erectile dysfunction. World J Mens Health 43: 28-40, 2025.

Copyright © 2026 Huang et al. This work is licensed under a Creative Commons Attribution-NonCommercial-NoDerivatives 4.0 International (CC BY-NC-ND 4.0) License.